Geophysical Journal International

Geophys. J. Int. (2016) **205,** 531–535
GJI Seismology

doi: 10.1093/gji/ggw023

EXPRESS LETTER

A single-sided homogeneous Green's function representation for holographic imaging, inverse scattering, time-reversal acoustics and interferometric Green's function retrieval

Kees Wapenaar, Jan Thorbecke and Joost van der Neut

Department of Geoscience and Engineering, Delft University of Technology, P.O. Box 5048, 2600 *GA Delft, The Netherlands.*
E-mail: c.p.a.wapenaar@tudelft.nl

Accepted 2016 January 15. Received 2016 January 12; in original form 2015 December 4

SUMMARY

Green's theorem plays a fundamental role in a diverse range of wavefield imaging applications, such as holographic imaging, inverse scattering, time-reversal acoustics and interferometric Green's function retrieval. In many of those applications, the homogeneous Green's function (i.e. the Green's function of the wave equation without a singularity on the right-hand side) is represented by a closed boundary integral. In practical applications, sources and/or receivers are usually present only on an open surface, which implies that a significant part of the closed boundary integral is by necessity ignored. Here we derive a homogeneous Green's function representation for the common situation that sources and/or receivers are present on an open surface only. We modify the integrand in such a way that it vanishes on the part of the boundary where no sources and receivers are present. As a consequence, the remaining integral along the open surface is an accurate single-sided representation of the homogeneous Green's function. This single-sided representation accounts for all orders of multiple scattering. The new representation significantly improves the aforementioned wavefield imaging applications, particularly in situations where the first-order scattering approximation breaks down.

Key words: Interferometry; Controlled source seismology; Wave scattering and diffraction.

1 INTRODUCTION

In optical, acoustic and seismic imaging, the central process is the retrieval of the wavefield inside the medium from experiments carried out at the boundary of that medium. Once the wavefield is known inside the medium, it can be used to form an image of the interior of that medium. The process to obtain the wavefield inside the medium is in essence a form of optical, acoustic or seismic holography (Porter 1970; Lindsey & Braun 2004). At the basis of these holographic methods lies Green's theorem, often cast in the form of a homogeneous Green's function representation or variants thereof. Although this representation is formulated as a closed boundary integral, measurements are generally available only on an open boundary. Despite this limitation, imaging methods based on the holographic principle work quite well in practice as long as the effects of multiple scattering are negligible. The same applies to linear inverse source problems (Porter & Devaney 1982) and linearized inverse scattering methods (Oristaglio 1989). However, in strongly inhomogeneous media the effects of multiple scattering can be quite severe. In these cases, approximating the closed boundary representation of the homogeneous Green's function by an open boundary integral leads to unacceptable errors in the homogeneous Green's function and, as a consequence, to significant artefacts in the image of the interior of the medium.

In the field of time-reversal acoustics, the response to a source inside a medium is recorded at the boundary of the medium, reversed in time and emitted back from the boundary into the medium. Because of the time-reversal invariance of the wave equation, the time-reversed field obeys the same wave equation as the original field and therefore focuses at the position of the source. The back-propagated field can be quantified by the homogeneous Green's function representation (Fink 2008). Time-reversed wavefield imaging (McMechan 1983) uses the same principle, except that here the time-reversed field is propagated numerically through a model of the medium. Time-reversal acoustics suffers from the same limitations as holographic imaging and inverse scattering: when the original field is recorded on an open boundary only, the back-propagated field is no longer accurately described by the homogeneous Green's function.

In the field of interferometric Green's function retrieval, the recordings of a wavefield at two receivers are mutually cross-correlated. Under specific conditions (equipartitioning of the wavefield, etc.), the time-dependent cross-correlation function converges to the response at one of the receivers to a virtual source at the position of the other, that is, the Green's function (Larose *et al.* 2006;

Schuster 2009). The method is related to time-reversed acoustics and hence the retrieved Green's function can be described by the homogeneous Green's function representation (Wapenaar & Fokkema 2006). When the positions of the primary sources are restricted to an open boundary, the retrieved Green's function may become very inaccurate.

The aim of this paper is to derive a single-sided homogeneous Green's function representation which circumvents the approximations inherent to the absence of sources/receivers on a large part of the closed boundary. We show that with our single-sided representation it is possible to obtain the complete response to a virtual source anywhere inside the medium, observed by virtual receivers anywhere inside the medium, from measurements on a single boundary (note that in our earlier work on the Marchenko method the response to the virtual source was only obtained for receivers at the surface).

2 THE CLASSICAL HOMOGENEOUS GREEN'S FUNCTION REPRESENTATION AND ITS APPLICATIONS

For the closed-boundary configuration of Fig. 1(a), the homogeneous Green's function representation for an arbitrary inhomogeneous lossless medium reads (Porter 1970; Oristaglio 1989; Wapenaar & Fokkema 2006)

$$G_{\rm h}(\mathbf{x}_A,\mathbf{x}_B,\omega) = \oint_{\partial\mathbb{D}} \frac{-1}{j\omega\rho(\mathbf{x})}\{G^*(\mathbf{x},\mathbf{x}_A,\omega)\partial_i G(\mathbf{x},\mathbf{x}_B,\omega) - \partial_i G^*(\mathbf{x},\mathbf{x}_A,\omega)G(\mathbf{x},\mathbf{x}_B,\omega)\}n_i \mathrm{d}^2\mathbf{x}, \quad (1)$$

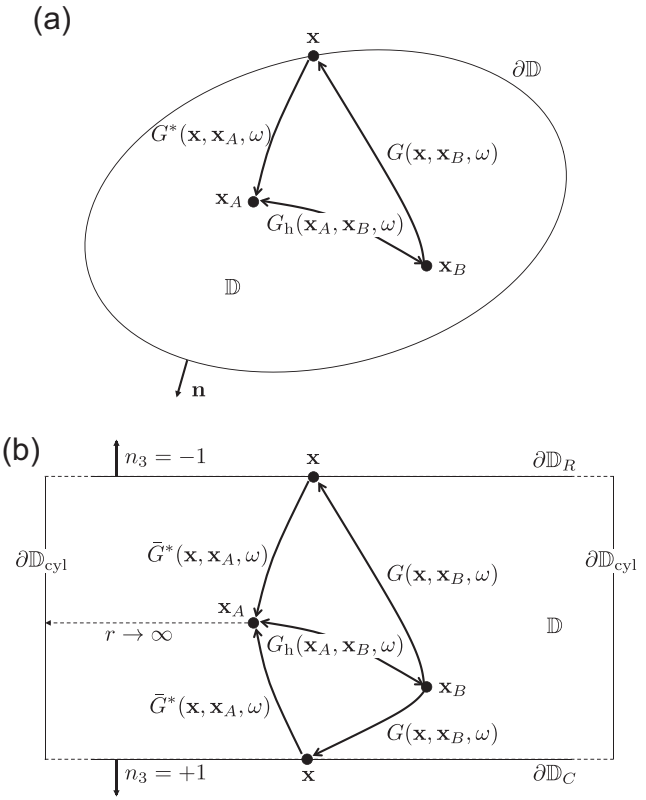

Figure 1. (a) Visualization of the homogeneous Green's function representation (eq. 1). Note that the rays in this figure represent the full responses between the source and receiver points, including multiple scattering. (b) Configuration for the modified representation. When the integrals along $\partial\mathbb{D}_C$ and $\partial\mathbb{D}_{\rm cyl}$ vanish, a single-sided representation remains.

where Green's function $G(\mathbf{x}, \mathbf{x}_B, \omega)$ is the frequency-domain response to a unit source at $\mathbf{x}_B$, observed at $\mathbf{x}$ (with ω denoting angular frequency), $G^*(\mathbf{x}, \mathbf{x}_A, \omega)$ (with the asterisk superscript denoting complex conjugation) is a back-propagating Green's function, and $G_{\rm h}(\mathbf{x}_A, \mathbf{x}_B, \omega) = G(\mathbf{x}_A, \mathbf{x}_B, \omega) + G^*(\mathbf{x}_A, \mathbf{x}_B, \omega) = 2\Re\{G(\mathbf{x}_A, \mathbf{x}_B, \omega)\}$ (with $\Re$ denoting the real part) is the homogeneous Green's function. Furthermore, $\rho(\mathbf{x})$ is the mass density, j the imaginary unit, ∂_i denotes differentiation with respect to x_i, and $\partial\mathbb{D}$ is a closed boundary with outward pointing normal vector $\mathbf{n} = (n_1, n_2, n_3)$; the domain enclosed by $\partial\mathbb{D}$ is denoted as $\mathbb{D}$. Einstein's summation convention applies to repeated subscripts. Another common form of the homogeneous Green's function is $\mathcal{G}_{\rm h}(\mathbf{x}_A, \mathbf{x}_B, \omega) = \mathcal{G}(\mathbf{x}_A, \mathbf{x}_B, \omega) - \mathcal{G}^*(\mathbf{x}_A, \mathbf{x}_B, \omega)$, with $\mathcal{G} = G/j\omega$. Further details about the derivation and different forms of the classical homogeneous Green's function representation can be found in the Supporting Information.

In imaging and inverse scattering applications, $G(\mathbf{x}, \mathbf{x}_B, \omega)$ in eq. (1) stands for measurements at the boundary $\partial\mathbb{D}$, $G^*(\mathbf{x}, \mathbf{x}_A, \omega)$ back-propagates these measurements to $\mathbf{x}_A$ inside the medium, and $G_{\rm h}(\mathbf{x}_A, \mathbf{x}_B, \omega)$ (fixed $\mathbf{x}_B$, variable $\mathbf{x}_A$) quantifies the resolution of the image around $\mathbf{x}_B$. For sufficiently large $\partial\mathbb{D}$ and a homogeneous medium outside $\partial\mathbb{D}$, eq. (1) can be approximated in the time domain by (Wapenaar & Fokkema 2006; Fink 2008)

$$G_{\rm h}(\mathbf{x}_B, \mathbf{x}_A, t) \approx \frac{2}{\rho c}\oint_{\partial\mathbb{D}} G(\mathbf{x}_B, \mathbf{x}, t) * G(\mathbf{x}, \mathbf{x}_A, -t)\mathrm{d}^2\mathbf{x}, \quad (2)$$

where t denotes time, c is the propagation velocity and the inline asterisk denotes temporal convolution. In time-reversal acoustics, $G(\mathbf{x}, \mathbf{x}_A, -t)$ is the time-reversed field injected from the boundary into the medium, $G(\mathbf{x}_B, \mathbf{x}, t)$ propagates this field to $\mathbf{x}_B$ inside the medium and $G_{\rm h}(\mathbf{x}_B, \mathbf{x}_A, t)$ (fixed $\mathbf{x}_A$, variable $\mathbf{x}_B$) describes the time-dependent evolution of the injected field through the medium. In interferometric Green's function retrieval, $G(\mathbf{x}_B, \mathbf{x}, t) * G(\mathbf{x}_A, \mathbf{x}, -t)$ describes the cross-correlation of measurements at $\mathbf{x}_B$ and $\mathbf{x}_A$ of responses to sources at the boundary, and the causal part of $G_{\rm h}(\mathbf{x}_B, \mathbf{x}_A, t)$ is the time-dependent response to a virtual source at $\mathbf{x}_A$, observed at $\mathbf{x}_B$.

3 AN AUXILIARY FUNCTION

In many practical cases, the medium of investigation can be approached from one side only. Hence, the exact closed boundary integral in eq. (1) is by necessity approximated by an open boundary integral, which leads to severe errors in the homogeneous Green's function, particularly when the medium is strongly inhomogeneous so that multiple scattering cannot be ignored. We consider a closed boundary $\partial\mathbb{D}$ which consists of three parts, according to $\partial\mathbb{D} = \partial\mathbb{D}_R \cup \partial\mathbb{D}_C \cup \partial\mathbb{D}_{\rm cyl}$, see Fig. 1(b). Here $\partial\mathbb{D}_R$ is the accessible boundary of the medium where the measurements take place. For simplicity we will assume it is a horizontal boundary, defined by $x_3 = x_{3,R}$. The second part of the closed boundary, $\partial\mathbb{D}_C$, is a horizontal boundary somewhere inside the medium, at which no measurements are done. This boundary is defined by $x_3 = x_{3,C}$, with $x_{3,C} > x_{3,R}$ (the positive x_3-axis is pointing downward). It is chosen sufficiently deep so that both $\mathbf{x}_A$ and $\mathbf{x}_B$ lie between $\partial\mathbb{D}_R$ and $\partial\mathbb{D}_C$. Finally, $\partial\mathbb{D}_{\rm cyl}$ is a cylindrical boundary with a vertical axis through $\mathbf{x}_A$ and infinite radius. This cylindrical boundary exists between $\partial\mathbb{D}_R$ and $\partial\mathbb{D}_C$ and closes the boundary $\partial\mathbb{D}$. The contribution of the integral over $\partial\mathbb{D}_{\rm cyl}$ vanishes (but for another reason than Sommerfeld's radiation condition, Wapenaar *et al.* (1989)).

We modify eq. (1) for this configuration as follows

$$G(\mathbf{x}_A, \mathbf{x}_B, \omega) + \bar{G}^*(\mathbf{x}_B, \mathbf{x}_A, \omega) = \int_{\partial\mathbb{D}_R} \frac{1}{j\omega\rho}\{\bar{G}_A^* \partial_3 G_B - \partial_3 \bar{G}_A^* G_B\}\mathrm{d}^2\mathbf{x} - \int_{\partial\mathbb{D}_C} \frac{1}{j\omega\rho}\{\bar{G}_A^* \partial_3 G_B - \partial_3 \bar{G}_A^* G_B\}\mathrm{d}^2\mathbf{x}, \quad (3)$$

where we used $\mathbf{n} = (0, 0, -1)$ on $\partial\mathbb{D}_R$ and $\mathbf{n} = (0, 0, +1)$ on $\partial\mathbb{D}_C$. $\bar{G}_A$ and G_B are short-hand notations for $\bar{G}(\mathbf{x}, \mathbf{x}_A, \omega)$ and $G(\mathbf{x}, \mathbf{x}_B, \omega)$, respectively. Note that we replaced $G(\mathbf{x}, \mathbf{x}_A, \omega)$ by a reference Green's function $\bar{G}(\mathbf{x}, \mathbf{x}_A, \omega)$, to be distinguished from the Green's function $G(\mathbf{x}, \mathbf{x}_B, \omega)$ in the actual medium. Both Green's functions obey the same wave equation in $\mathbb{D}$ (with different source positions), but at and outside $\partial\mathbb{D} = \partial\mathbb{D}_R \cup \partial\mathbb{D}_C$ the medium parameters for these Green's functions may be different (Wapenaar *et al.* 1989). For the Green's function $\bar{G}(\mathbf{x}, \mathbf{x}_A, \omega)$ we choose a reference medium which is identical to the actual medium below $\partial\mathbb{D}_R$, but homogeneous at and above $\partial\mathbb{D}_R$.

Next, at $\partial\mathbb{D}_C$ we choose boundary conditions in such a way that the integral along $\partial\mathbb{D}_C$ vanishes. Imposing either a Dirichlet or a Neumann boundary condition is not sufficient because when $\bar{G}(\mathbf{x}, \mathbf{x}_A, \omega)$ is zero on $\partial\mathbb{D}_C$ then $\partial_3\bar{G}(\mathbf{x}, \mathbf{x}_A, \omega)$ is not, and vice versa. Hence, $\bar{G}(\mathbf{x}, \mathbf{x}_A, \omega)$ cannot obey Dirichlet and Neumann conditions simultaneously. To deal with this problem, we introduce an auxiliary function $\Gamma(\mathbf{x}, \omega)$ which we subtract from the reference Green's function, according to

$$\bar{G}(\mathbf{x}, \mathbf{x}_A, \omega) \rightarrow \bar{G}(\mathbf{x}, \mathbf{x}_A, \omega) - \Gamma(\mathbf{x}, \omega). \quad (4)$$

The function $\Gamma(\mathbf{x}, \omega)$ is defined in the reference medium and obeys the same wave equation as $\bar{G}(\mathbf{x}, \mathbf{x}_A, \omega)$, but without the singularity at $\mathbf{x}_A$. As a consequence, $\bar{G}(\mathbf{x}, \mathbf{x}_A, \omega) - \Gamma(\mathbf{x}, \omega)$ obeys the same wave equation as $\bar{G}(\mathbf{x}, \mathbf{x}_A, \omega)$, with the singularity at $\mathbf{x}_A$. Hence, in eq. (3) we may replace $\bar{G}(\mathbf{x}, \mathbf{x}_A, \omega)$ by $\bar{G}(\mathbf{x}, \mathbf{x}_A, \omega) - \Gamma(\mathbf{x}, \omega)$, according to

$$G(\mathbf{x}_A, \mathbf{x}_B, \omega) + \{\bar{G}(\mathbf{x}_B, \mathbf{x}_A, \omega) - \Gamma(\mathbf{x}_B, \omega)\}^* = \int_{\partial\mathbb{D}_R} \frac{1}{j\omega\rho}\{(\bar{G}_A - \Gamma)^* \partial_3 G_B - \partial_3(\bar{G}_A - \Gamma)^* G_B\}\mathrm{d}^2\mathbf{x} - \int_{\partial\mathbb{D}_C} \frac{1}{j\omega\rho}\{(\bar{G}_A - \Gamma)^* \partial_3 G_B - \partial_3(\bar{G}_A - \Gamma)^* G_B\}\mathrm{d}^2\mathbf{x}. \quad (5)$$

When a function $\Gamma(\mathbf{x}, \omega)$ can be found such that $\bar{G}(\mathbf{x}, \mathbf{x}_A, \omega) - \Gamma(\mathbf{x}, \omega)$ obeys the Cauchy boundary condition (i.e. simultaneous Dirichlet and Neumann boundary conditions) on $\partial\mathbb{D}_C$, then the integral along $\partial\mathbb{D}_C$ vanishes.

Introducing auxiliary functions is a common approach to manipulate the boundary conditions (Morse & Feshbach 1953; Berkhout 1982). In fact it has been previously proposed for the integral in eq. (5) (Weglein *et al.* 2011), but a straightforward way to find a $\Gamma(\mathbf{x}, \omega)$ that obeys the conditions for an arbitrary inhomogeneous medium has, to the knowledge of the authors, not been presented yet. Recent work of the authors (Wapenaar *et al.* 2014) concerns the generalization of the single-sided 1-D Marchenko method for inverse scattering (Marchenko 1955) and autofocusing (Rose 2002; Broggini & Snieder 2012) to the 3-D situation. We show with intuitive arguments that the so-called focusing functions, developed for the single-sided 3-D Marchenko method, provide a means to find $\Gamma(\mathbf{x}, \omega)$. For a more precise derivation we refer to the Supporting Information.

Fig. 2(a) shows a focusing function $f_1^+(\mathbf{x}, \mathbf{x}_A, \omega)$ (downward pointing red rays), which is emitted from the homogeneous upper half-space into the medium to focus at $\mathbf{x}_A$. Because there is no sink at $\mathbf{x}_A$ to annihilate the focused field $f_1^+(\mathbf{x}_A, \mathbf{x}_A, \omega)$, the field continues to propagate as if there were a source for downgoing waves at $\mathbf{x}_A$ (indicated by the green rays). The response to this virtual downward radiating source mimics a part of the Green's function $\bar{G}(\mathbf{x}, \mathbf{x}_A, \omega)$. We now discuss how the remaining part of the Green's function is obtained. Before reaching the focus, a part of the focusing function is reflected upward and is called $f_1^-(\mathbf{x}, \mathbf{x}_A, \omega)$ (upward pointing blue rays in Fig. 2(a)). Fig. 2(b) visualizes the emission of the back-propagating focusing function $-\{f_1^-(\mathbf{x}, \mathbf{x}_A, \omega)\}^*$ into the medium (downward pointing red rays). Its response consists of $-\{f_1^+(\mathbf{x}, \mathbf{x}_A, \omega)\}^*$ (upward pointing blue rays), and a field apparently originating from a source for upgoing waves at $\mathbf{x}_A$ (indicated by the green rays). The response to this virtual upward radiating source mimics the remaining part of the Green's function $\bar{G}(\mathbf{x}, \mathbf{x}_A, \omega)$. Figs 2(a) and (b) together visualize the auxiliary function $\Gamma(\mathbf{x}, \omega)$. It consists of the Green's function $\bar{G}(\mathbf{x}, \mathbf{x}_A, \omega)$ (the green rays in both figures) and, above the focal point, the focusing function $f_1(\mathbf{x}, \mathbf{x}_A, \omega) - \{f_1(\mathbf{x}, \mathbf{x}_A, \omega)\}^*$, with $f_1(\mathbf{x}, \mathbf{x}_A, \omega) = f_1^+(\mathbf{x}, \mathbf{x}_A, \omega) + f_1^-(\mathbf{x}, \mathbf{x}_A, \omega)$ (the red and blue rays). Hence,

$$\Gamma(\mathbf{x}, \omega) = \bar{G}(\mathbf{x}, \mathbf{x}_A, \omega) + H(x_{3,A} - x_3)2j\Im\{f_1(\mathbf{x}, \mathbf{x}_A, \omega)\}, \quad (6)$$

where $H(x_3)$ is the Heaviside step function and $\Im$ denotes the imaginary part. With this definition, $\bar{G}(\mathbf{x}, \mathbf{x}_A, \omega) - \Gamma(\mathbf{x}, \omega)$ vanishes in

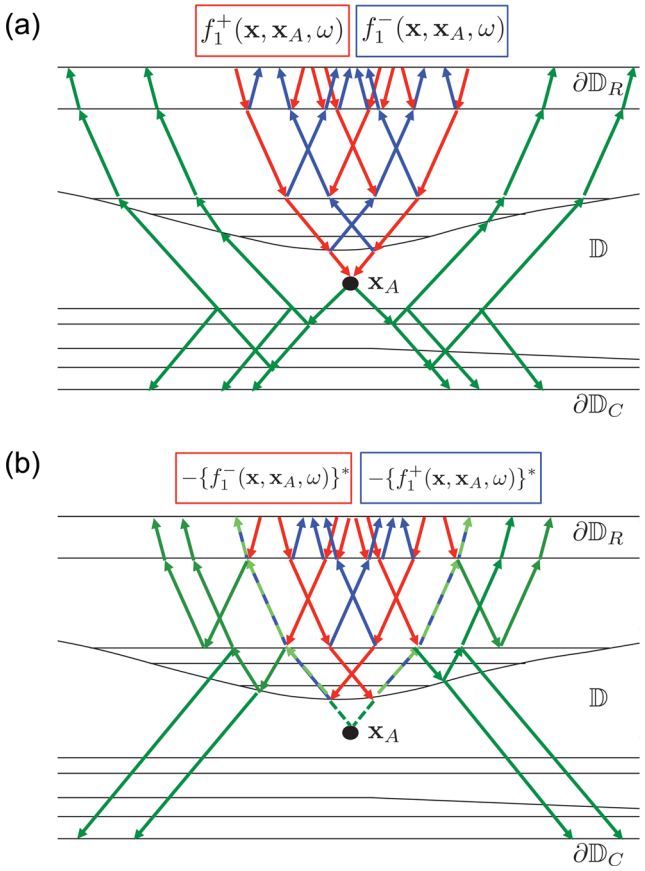

Figure 2. Visualization of the auxiliary function $\Gamma(\mathbf{x}, \omega)$. It consists of the focusing functions $f_1^{\pm}(\mathbf{x}, \mathbf{x}_A, \omega)$ and $-\{f_1^{\mp}(\mathbf{x}, \mathbf{x}_A, \omega)\}^*$ (red and blue rays) and the Green's function $\bar{G}(\mathbf{x}, \mathbf{x}_A, \omega)$ (green rays). By subtracting this auxiliary function from the Green's function (eq. 4), the field in the half-space below $\mathbf{x}_A$ vanishes and hence obeys the Cauchy boundary condition at $\partial\mathbb{D}_C$.

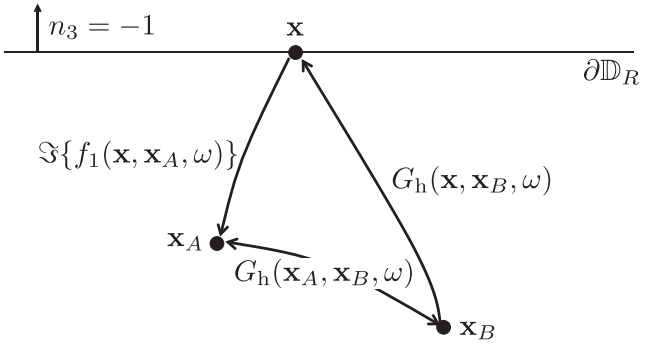

Figure 3. Visualization of the single-sided homogeneous Green's function representation (eq. 8). Similar as in Fig. 1, the rays in this figure represent the full responses between the source and receiver points, including multiple scattering.

the half-space below $\mathbf{x}_A$. Because this function is zero in an entire half-space, its derivative is zero as well and hence it obeys the Cauchy boundary condition at $\partial\mathbb{D}_C$.

4 THE SINGLE-SIDED HOMOGENEOUS GREEN'S FUNCTION REPRESENTATION

Substitution of eq. (6) into eq. (5) gives

$$G(\mathbf{x}_A, \mathbf{x}_B, \omega) + H(x_{3,A} - x_{3,B})2j\Im\{f_1(\mathbf{x}_B, \mathbf{x}_A, \omega)\} = \int_{\partial\mathbb{D}_R} \frac{2}{\omega\rho(\mathbf{x})}\Big(\Im\{f_1(\mathbf{x}, \mathbf{x}_A, \omega)\}\partial_3 G(\mathbf{x}, \mathbf{x}_B, \omega) - \Im\{\partial_3 f_1(\mathbf{x}, \mathbf{x}_A, \omega)\}G(\mathbf{x}, \mathbf{x}_B, \omega)\Big)\mathrm{d}^2\mathbf{x}. \quad (7)$$

Taking the real part of both sides of this equation gives

$$G_{\rm h}(\mathbf{x}_A, \mathbf{x}_B, \omega) = \int_{\partial\mathbb{D}_R} \frac{2}{\omega\rho(\mathbf{x})}\Big(\Im\{f_1(\mathbf{x}, \mathbf{x}_A, \omega)\}\partial_3 G_{\rm h}(\mathbf{x}, \mathbf{x}_B, \omega) - \Im\{\partial_3 f_1(\mathbf{x}, \mathbf{x}_A, \omega)\}G_{\rm h}(\mathbf{x}, \mathbf{x}_B, \omega)\Big)\mathrm{d}^2\mathbf{x}. \quad (8)$$

This is the main result of this paper. The homogeneous Green's function $G_{\rm h}(\mathbf{x}_A, \mathbf{x}_B, \omega)$, with both $\mathbf{x}_A$ and $\mathbf{x}_B$ inside the medium, is represented by an integral along the acquisition boundary $\partial\mathbb{D}_R$ only (Fig. 3).

Note that the Green's function $G_{\rm h}(\mathbf{x}, \mathbf{x}_B, \omega)$ under the integral can be obtained from a similar representation. With some simple replacements (see Supporting Information for details) we obtain

$$G_{\rm h}(\mathbf{x}, \mathbf{x}_B, \omega) = \int_{\partial\mathbb{D}_S} \frac{2}{\omega\rho(\mathbf{x}')}\Big(\Im\{f_1(\mathbf{x}', \mathbf{x}_B, \omega)\}\partial'_3 G_{\rm h}(\mathbf{x}, \mathbf{x}', \omega) - \Im\{\partial'_3 f_1(\mathbf{x}', \mathbf{x}_B, \omega)\}G_{\rm h}(\mathbf{x}, \mathbf{x}', \omega)\Big)\mathrm{d}^2\mathbf{x}', \quad (9)$$

with $\mathbf{x}$ on $\partial\mathbb{D}_R$ and $\mathbf{x}'$ on $\partial\mathbb{D}_S$, just above $\partial\mathbb{D}_R$. Note that $G_{\rm h}(\mathbf{x}, \mathbf{x}', \omega)$ stands for the reflection response at the surface. Hence, eqs (8) and (9) can be used to retrieve $G_{\rm h}(\mathbf{x}_A, \mathbf{x}_B, \omega)$ from $G(\mathbf{x}, \mathbf{x}', \omega)$ in a data-driven way. The complete procedure is as follows. Define the initial estimate of the focusing function $f_1(\mathbf{x}', \mathbf{x}_B, \omega)$ by the time-reversed direct arrivals between $\mathbf{x}_B$ and $\mathbf{x}'$ at the boundary. Retrieve the complete focusing function $f_1(\mathbf{x}', \mathbf{x}_B, \omega)$ from its initial estimate and the reflection response $G(\mathbf{x}, \mathbf{x}', \omega)$ at the surface, using the iterative Marchenko method (Wapenaar *et al.* 2014). Use eq. (9) to obtain $G_{\rm h}(\mathbf{x}, \mathbf{x}_B, \omega)$ from $G_{\rm h}(\mathbf{x}, \mathbf{x}', \omega)$. This step brings the sources down from $\mathbf{x}'$ on $\partial\mathbb{D}_S$ to $\mathbf{x}_B$. Next, in a similar way use eq. (8) to obtain $G_{\rm h}(\mathbf{x}_A, \mathbf{x}_B, \omega)$ from $G_{\rm h}(\mathbf{x}, \mathbf{x}_B, \omega)$. This step brings the receivers down from $\mathbf{x}$ on $\partial\mathbb{D}_R$ to $\mathbf{x}_A$.

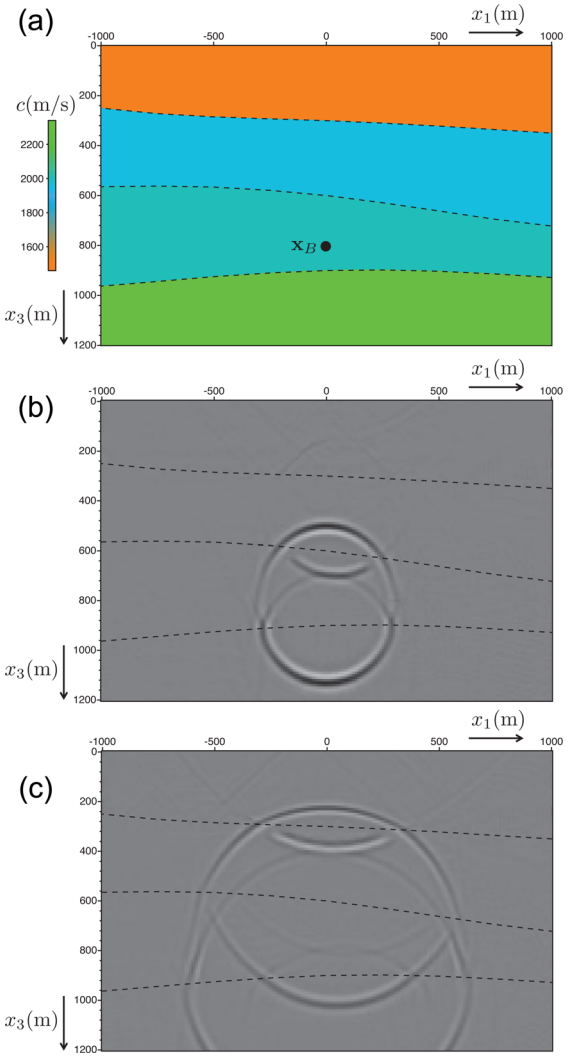

Figure 4. Numerical example, illustrating the application of the single-sided homogeneous Green's function representations (eqs 8 and 9). (a) Inhomogeneous medium. (b) Snapshot of $G(\mathbf{x}_A, \mathbf{x}_B, t) + G(\mathbf{x}_A, \mathbf{x}_B, -t)$ at $t = 0.15$ s, for fixed $\mathbf{x}_B = (0, 800)$ and variable $\mathbf{x}_A$. (c) Idem, for $t = 0.30$ s.

Recall that the Green's functions without bars are defined in the actual medium, which may be inhomogeneous above $\partial\mathbb{D}_R$. For example, similar as discussed by Singh *et al.* (2015), there may be a free boundary just above $\partial\mathbb{D}_R$, in which case the second term under the integral in eqs (7)–(9) vanishes. In the following example, however, the half-space above $\partial\mathbb{D}_R$ is homogeneous. Fig. 4(a) shows a 2D inhomogeneous medium. We modelled the reflection response $G(\mathbf{x}, \mathbf{x}', \omega)$ for 600 sources and 600 receivers, with a horizontal spacing of 10 m, at the upper boundary. The central frequency of the band-limited source function is 30 Hz. Using the process described above we obtain $G_{\rm h}(\mathbf{x}_A, \mathbf{x}_B, \omega)$, or in the time domain $G_{\rm h}(\mathbf{x}_A, \mathbf{x}_B, t) = G(\mathbf{x}_A, \mathbf{x}_B, t) + G(\mathbf{x}_A, \mathbf{x}_B, -t)$. The Supporting Information contains a movie of $G_{\rm h}(\mathbf{x}_A, \mathbf{x}_B, t)$ for $t \geq 0$. Figs 4(b)–(c) show 'snapshots' of this function for $t = 0.15$ s and $t = 0.30$ s, respectively, each time for fixed $\mathbf{x}_B = (0, 800)$ and variable $\mathbf{x}_A$. Note that the movie and snapshots nicely mimic the response to a source at $\mathbf{x}_B = (0, 800)$, including scattering at the interfaces between

layers with different propagation velocities. It is remarkable that this virtual response is obtained from the reflection response at the upper boundary plus estimates of the direct arrivals, but no information about the positions and shapes of the scattering interfaces has been used. Yet the virtual response clearly shows how scattering occurs at the interfaces.

5 DISCUSSION

Unlike the classical homogeneous Green's function representation (eq. 1), the single-sided representation of eq. (8) can be applied in situations in which the medium of investigation is accessible from one side only. We foresee many interesting applications, which we briefly indicate below.

Eq. (8) will find its most prominent applications in holographic imaging and inverse scattering in strongly inhomogeneous media. As illustrated in the previous section, the two-step procedure described by eqs (8) and (9) brings sources and receivers down from the surface to arbitrary positions in the subsurface. For weakly scattering media (ignoring multiples), a similar two-step process is known in exploration seismology as source–receiver redatuming (Berkhout 1982; Berryhill 1984). For strongly scattering media (including multiple scattering) a similar two-step process, called source–receiver interferometry, has previously been formulated in terms of closed-boundary representations for the homogeneous Green's function (Halliday & Curtis 2010). Our method replaces the closed boundary representations in the latter method by single-sided representations. Once $G_{\rm h}(\mathbf{x}_A, \mathbf{x}_B, \omega)$ is obtained, an image can be formed by setting $\mathbf{x}_A$ equal to $\mathbf{x}_B$. However, $G_{\rm h}(\mathbf{x}_A, \mathbf{x}_B, t)$ for variable and independent virtual sources and receivers contains a wealth of additional information about the interior of the medium, as can be witnessed from Fig. 4. The advantages of the two-step process for holographic imaging and inverse scattering will be further explored. Results like that in Fig. 4 could for example also be used to predict the propagation of microseismic signals through an unknown subsurface.

For the field of time-reversal acoustics, the inverse Fourier transform of eq. (7) forms an alternative to eq. (2). It shows that, instead of physically injecting $G(\mathbf{x}, \mathbf{x}_A, -t)$ from a closed boundary into the medium, the function $f_1(\mathbf{x}, \mathbf{x}_A, t) - f_1(\mathbf{x}, \mathbf{x}_A, -t)$ should be injected into the medium when it is accessible only from one side. The injected field will focus at $\mathbf{x}_A$ and subsequently the focused field will act as a virtual source.

The application of eq. (8) for interferometric Green's function retrieval is very similar to the redatuming procedure described above. However, in the field of seismic interferometry the Green's functions $G(\mathbf{x}_A, \mathbf{x}, t)$ and $G(\mathbf{x}_B, \mathbf{x}, t)$ usually stand for measured data. This has the potential to obtain a more accurate estimate of the focusing function $f_1(\mathbf{x}, \mathbf{x}_A, t)$. Substituting its Fourier transform into eq. (8), together with that of the measured response $G(\mathbf{x}_B, \mathbf{x}, t)$, may yield an even more accurate recovery of the homogeneous Green's function.

We foresee that the single-sided representation of the homogeneous Green's function will lead to many more applications in holographic imaging, inverse scattering, time-reversal acoustics and interferometric Green's function retrieval.

ACKNOWLEDGEMENTS

We thank Dirk-Jan van Manen and an anonymous reviewer for their constructive reviews and for challenging us to improve the explanation of the theory.

REFERENCES

Berkhout, A.J., 1982. *Seismic Migration. Imaging of Acoustic Energy by Wave Field Extrapolation. A. Theoretical Aspects,* Elsevier.

Berryhill, J.R., 1984. Wave-equation datuming before stack, *Geophysics,* **49,** 2064–2066.

Broggini, F. & Snieder, R., 2012. Connection of scattering principles: a visual and mathematical tour, *Eur. J. Phys.,* **33,** 593–613.

Fink, M., 2008. Time-reversal acoustics, *J. Phys.: Conf. Ser.,* **118,** 012001.

Halliday, D. & Curtis, A., 2010. An interferometric theory of source-receiver scattering and imaging, *Geophysics,* **75**(6), SA95–SA103.

Larose, E. *et al.*, 2006. Correlation of random wave fields: an interdisciplinary review, *Geophysics,* **71**(4), SI11–SI21.

Lindsey, C. & Braun, D.C., 2004. Principles of seismic holography for diagnostics of the shallow subphotosphere, *Astrophys. J. Suppl. Ser.,* **155**(1), 209–225.

Marchenko, V.A., 1955. Reconstruction of the potential energy from the phases of the scattered waves (in Russian), *Dokl. Akad. Nauk SSSR,* **104**(5), 695–698.

McMechan, G.A., 1983. Migration by extrapolation of time-dependent boundary values, *Geophys. Prospect.,* **31,** 413–420.

Morse, P.M. & Feshbach, H., 1953. *Methods of Theoretical Physics,* Vol. I, McGraw-Hill Book Company Inc.

Oristaglio, M.L., 1989. An inverse scattering formula that uses all the data, *Inverse Probl.,* **5,** 1097–1105.

Porter, R.P., 1970. Diffraction-limited, scalar image formation with holograms of arbitrary shape, *J. Opt. Soc. Am.,* **60,** 1051–1059.

Porter, R.P. & Devaney, A.J., 1982. Holography and the inverse source problem, *J. Opt. Soc. Am.,* **72,** 327–330.

Rose, J.H., 2002. 'Single-sided' autofocusing of sound in layered materials, *Inverse Probl.,* **18,** 1923–1934.

Schuster, G.T., 2009. *Seismic Interferometry,* Cambridge Univ. Press.

Singh, S., Snieder, R., Behura, J., van der Neut, J., Wapenaar, K. & Slob, E., 2015. Marchenko imaging: imaging with primaries, internal multiples, and free-surface multiples, *Geophysics,* **80**(5), S165–S174.

Wapenaar, K. & Fokkema, J., 2006. Green's function representations for seismic interferometry, *Geophysics,* **71**(4), SI33–SI46.

Wapenaar, C.P.A., Peels, G.L., Budejicky, V. & Berkhout, A.J., 1989. Inverse extrapolation of primary seismic waves, *Geophysics,* **54**(7), 853–863.

Wapenaar, K., Thorbecke, J., van der Neut, J., Broggini, F., Slob, E. & Snieder, R., 2014. Marchenko imaging, *Geophysics,* **79**(3), WA39–WA57.

Weglein, A.B., Stolt, R.H. & Mayhan, J.D., 2011. Reverse time migration and Green's theorem: Part II - A new and consistent theory that progresses and corrects current RTM concepts and methods, *J. Seism. Explor.,* **20,** 135–159.

SUPPORTING INFORMATION

Additional Supporting Information may be found in the online version of this paper:

Appendix 1. Derivation of the classical homogeneous Green's function representation.
Appendix 2. Derivation of the auxiliary function.
Appendix 3. Alternative derivation of the single-sided representation.
Movie 1. The homogeneous Green's function $G_{\rm h}(\mathbf{x}_A, \mathbf{x}_B, t)$ for $t \geq 0$, obtained from the reflection response at the upper boundary.
Movie 2. As a reference, the Green's function $G(\mathbf{x}_A, \mathbf{x}_B, t)$ obtained by direct modelling.
(http://gji.oxfordjournals.org/lookup/suppl/doi:10.1093/gji/ggw023/-/DC1).

Please note: Oxford University Press is not responsible for the content or functionality of any supporting materials supplied by the authors. Any queries (other than missing material) should be directed to the corresponding author for the paper.